ELSEVIER

Nuclear Instruments and Methods in Physics Research B 168 (2000) 1–10

NIM B
Beam Interactions with Materials & Atoms

www.elsevier.nl/locate/nimb

Multiple scattering measurements of energetic positrons in a thin gold polycrystal

F.A. Selim [a,*], A.W. Hunt [a,b], R. Howell [a], K.G. Lynn [c], J.A. Golovchenko [b,d]

[a] *Lawrence Livermore National Laboratory, Livermore, CA 94551, USA*
[b] *Department of Physics, Harvard University, Cambridge, MA 02138, USA*
[c] *Department of Physics, Washington State University, Pullman, WA 99164, 2814, USA*
[d] *Rowland Institute for Science, Cambridge, MA 02142, USA*

Received 18 June 1999

Abstract

As a step towards developing fast positrons as a probe to measure electron density and spin magnetic density in crystals, an experiment has been performed to measure the multiple scattering distribution of MeV positrons penetrating through thin polycrystalline films in both random and channeling directions. Image plate detectors were used to determine the angular distribution of emergent positrons. Image plate sensitivity was measured for high-energy positrons and for the background radiation encountered in our experiment. The image plates showed good sensitivity and good linearity for MeV positrons. The multiple scattering results are compared with the theory for random direction and show disagreement due to crystal effects and quantum mechanical considerations.

PACS: 34.85.+x; 11.80.La
Keywords: Positron scattering; Multiple scattering; Channeling; Image plate detector

1. Introduction

Multiple scattering theories [1,2] are often used to describe penetration of MeV electrons and positrons through random media or crystalline media in random directions. It is not completely clear how reliable they are for positron penetration in crystals where correlation between collisions is not taken into account and the use of classical orbital picture [3] is implied. There is also lack of experimental results for the electron and positron multiple scattering. Few experiments [4,5] have been performed in the past to measure the multiple scattering of MeV electrons in random targets only. We are not aware of any reports of multiple scattering measurements for MeV positrons. Furthermore the attempt to use fast positrons as a

* Corresponding author. Address: Department of Engineering Physics, Faculty of Engineering, Alexandria University, Alexandria 21544, Egypt. Tel.: +203-545-1235; fax: +203-597-1853.

E-mail addresses: selim@huhepu.harvard.edu, faselim@yahoo.com (F.A. Selim).

0168-583X/00/$ - see front matter
PII: S0168-583X(99)00718-1

probe in solid state and materials science requires complete understanding of positron scattering in crystals.

The prospect of using single quantum annihilation (SQA) and two quantum annihilation (TQA) in flight of MeV channeled positrons in thin crystalline films to determine electron and spin densities has been discussed in detail [6,7]. A main difficulty in the technique arises from the low cross-section for in flight SQA and TQA. The yield of channeling annihilation events is increased by increasing the thickness of the crystal, but this also leads to enhanced positron multiple scattering, which can seriously complicate the interpretation of the data. For random directions of incidence, the positrons experience enhanced multiple scattering, inducing significant background due to the annihilation of multiple scattered positrons in the chamber walls. In addition the multiple scattering of positrons within the crystal causes an increase in the directional divergence of the detected SQA and TQA radiation. Well-channeled positrons occupy the middle of the channel far away from the nuclei and they are multiply scattered by the valence electrons only. Electronic multiple scattering results in a decrease in the fraction of the channeled positrons.

We performed an experiment to measure the angular distributions of 2.8 MeV positrons transmitted through a 1.67 μm gold crystal in both random and channeling directions. The measured distributions in the random direction have been compared with multiple scattering theories. One of our objectives here is to reveal the extent to which such theories agree with experiments in crystals when channeling effects are absent. The comparisons do show significant disagreement. The discrepancy between the theory and the experiment will be discussed on a basis of crystal and interference effects.

We also report in this work the characteristics of the image plates as a sensistive detector for MeV positrons. The imaging plates (IPs) were first developed as a detector for X-ray diagnostics [8] and then were developed for transmission electron microscopy [9]. Their response was tested up to few keV energies only [10,11]. The plates are read out by laser scanning. They have wide dynamic range, linear response, high sensitivity and resolution. We tested the performance of the IP for MeV positrons. The calibration measurements showed the same characteristics for positron detection, with good sensitivity even at MeV energies. The measurements also showed that the plates are not sensitive to the 511 keV gamma radiation commonly encountered in positron annihilation experiments. We were therefore successfully able to measure the angular distributions of positrons behind the gold crystals using IPs.

2. Experiment set-up

The experiment was conducted at the Lawrence Livermore National Laboratory (LLNL) positron facility. The accelerator and beam line are illustrated in Fig. 1. Positrons emitted from a ^{22}Na source of strength ~50 mCi are incident on a

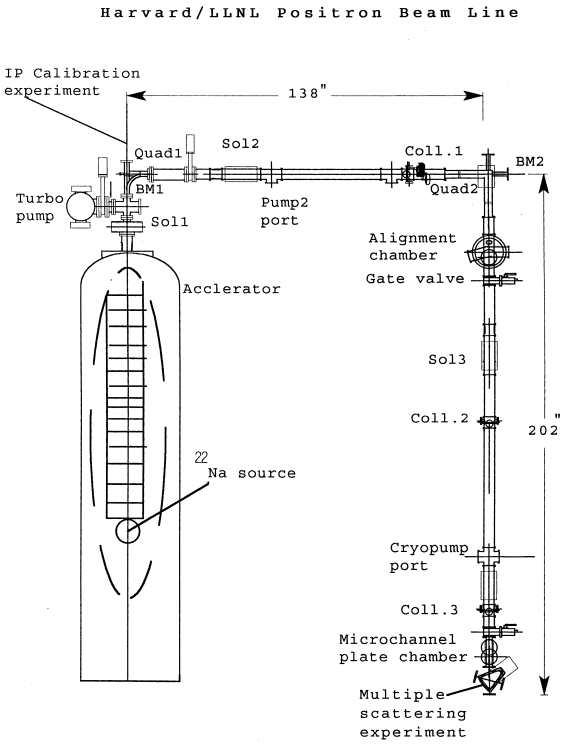

Fig. 1. A schematic drawing of the beam line, dimensions in inch.

W(1 0 0) transmission moderator [12]. The thermalized positrons emitted by the moderator are accelerated in a modified NEC Pelletron to 2.8 MeV. We performed two experiments. One tested and calibrated the IP detector for MeV positrons and in the other we measured the multiple scattering of MeV positrons penetrating through gold crystals.

The calibration measurements of the IP were performed at the unanalyzed output of the accelerator as shown in Fig. 1, when a beam of 4.0×10^5 moderated and unmoderated e^+/s is available. A solenoid is used to focus the beam to 5 mm spot through a small 5 mm thick Al window, where we exposed the IPs. The positrons were counted with a scintiallator and the beam size was checked using Polaroid film.

2.1. Image plate detector and calibration measurements

The image plate (IP) is a reusable flexible sheet made of photostimulable phosphor (BaFX, X = Cl, Br, I) doped with Eu^{2+}. It is covered with a protective layer on the front side and has a support material and a light shield on the backside. The detection mechanism is described as follows [11]. When electrons penetrate the phosphor, electron–hole pairs are created. Some of the secondary electrons are trapped at the defects of the phosphor and the holes are trapped at Eu^{2+} giving Eu^{3+}. The recorded image plate is read out by a scanning laser beam that excites the trapped electrons, which recombine to yield Eu^{2+}. Light is emitted when the excited Eu^{2+} returns to its ground state. The luminescence photons are guided to a photomultiplier tube and counted. We used Fuji FDL 5000 image plates, size (99.6 × 80.9 mm) with 24 μm pixel size. The plates were sent to the Solid State Science Facility at Arizona State University where they were read by the commercial (Fuji FDL 5000) reader [11].

Fig. 2 shows the sensitivity of the IP as a function of dose for 2.8 MeV positrons. The signal intensity represents the number of positrons detected per pixel. The response of the IP is quite linear and the dynamic range covers three decades.

The dependence of sensitivity on electron energy was measured to 400 keV by Mori et al. [10] for a 50 μm pixel IP, and by Zuo et al. [11] for a 25 μm pixel IP. They showed the highest sensitivity at about 150 keV which then decreases with increasing energy. We measured the sensitivity of the IP at higher positron energies ranging from 1 to 2.8 MeV. The sensitivity dependence on positron

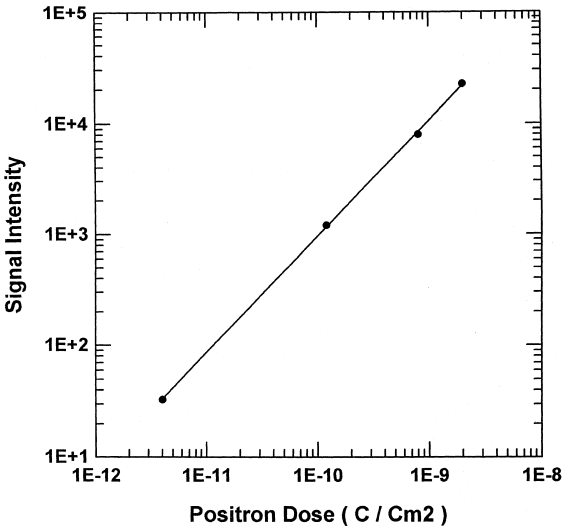

Fig. 2. Response of IP as a function of positron dose.

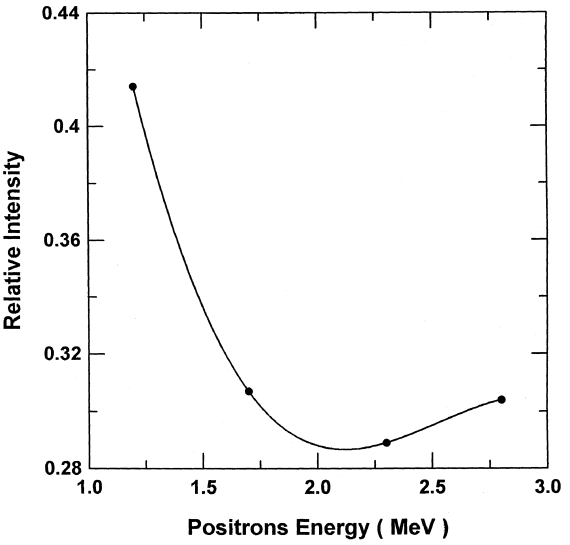

Fig. 3. Dependence of IP sensitivity on positron energy.

energy at positron dose 2.4×10^{-10} c/cm^2 is shown in Fig. 3. The relative intensity represents the number of positrons detected per pixel normalized to the incident positron beam.

The decrease in sensitivity below 150 keV is due to the reduction of the electron energy and the energy deposited by the incident electron in the protective layer which does not contribute to the exposure of the plate. Since the phosphor layer is thin (110 μm thick for 25 μm pixel IP), the decrease of sensitivity with increasing energy just above 150 keV is due to the electrons range exceeding the active layer thickness. We should also mention that only about 80% of this thickness is sensitive because the laser beam is absorbed and diffused through the phosphor and its intensity becomes small at the deep part of the phosphor [10]. The range of 200 keV electrons in the phosphor is about 81, and about 232 μm for 400 keV electrons based on equations from [13] using the phosphor density of 5.14 gm/cm^2 [9]. Thus, above 200 keV, the decrease of sensitivity is due to the decrease of the ionization energy loss (dE/dx) of electrons with increasing energy up to 500 keV. Above 500 keV dE/dx decreases but very slightly with the electron energy up to 2 MeV and then it goes up due to the density effect [14].

Some measurements have been performed to test the sensitivity of the IP to the background. First, 400,000 e^+/s were stopped in a sheet of lead, and an IP was exposed to the 511 gamma radiation emitted from it for 4 h. No significant signal was recorded. Since the IP target chamber for the multiple scattering experiments is facing the accelerator with the radioactive source inside it as shown in Fig. 1, there is a significant background in the vicinity of the IP due to the annihilation of positrons, Bremsstrahlung radiation, and accelerator related background. We measured the background around the multiple scattering experiment when the accelerator was running using NaI detector and HPGe detectors. The measurements showed background with a wide spectrum from few keV to few MeV. The IP is sensitive to the low energy photons mainly because the X-ray absorption coefficient in the phosphor reaches a maximum at about 5 keV [15] and goes down with increasing energy to about 1% of the maximum at 200 keV. The ratio of the background to the signal detected on the IP is about 10% in the average for the presented results. Perhaps in experiments when the background is serious, having a combination shielding of lead, copper and aluminium around the IP chamber can reduce the background to a low level.

2.2. Sample preparation and crystal quality

The Au crystals were prepared at Aarhus Univerisity in Denmark using evaporation technique on NaCl substrates. They were expected to be nominally of ⟨1 0 0⟩ orientation. We performed proton channeling measurements on the crystals at the Harvard CAMS facility to test their quality. The minimum yield χ_{min} [16] is a good indicator of the overall quality of single crystals. Backscattering energy spectra for 2 MeV protons were measured in both random and channeling directions. They showed a χ_{min} of 50–60%. The crystal thickness was also established to be 1.67 μm.

For high quality single crystal samples, χ_{min}s of 5% are expected. The extremely high χ_{min} we measured reflects a crystal quality well below that needed for serious channeling studies but should be fine for our multiple scattering studies when a good random direction is chosen. The 40% minimum yield could not arise from conventional defects such as point or line defects. The most likely cause of the high dechanneling rate in our samples is twinning. A twin is a region in the crystal that has a different but distinct orientation relative to the original crystal orientation. In these regions, the beam exhibits higher dechanneling rates. Au (1 0 0) crystals prepared by evaporation methods (the same method we used in preparing our crystals) have been studied in the past by electron microscopy [17]. The samples can contain many microtwins on the four {1 1 1} planes. By going from untwined to twinned regions, the crystal axes are converted by 180° rotation about the [1 0 0] twin axes. The nominal ⟨1 0 0⟩ axis normal to the surface is converted to high index ⟨2 2 1⟩ axis and the dechanneling is greatly enhanced. The detailed process used to prepare our samples is proprietary and known to usually yield high quality single crystals but we believe twinning to be the origin of

50% χ_{min} in this case. Further studies of our samples were not possible due to damage during transportation. Consequently we characterize our samples as polycrystalline. We know of no technique to create truly amorphous glass like gold samples.

2.3. Multiple scattering measurements

The multiple scattering experiment was performed at the end of a beam line constructed for the positron channeling annihilation in flight experiments [7]. The beam line is shown in Fig. 1. The beam goes through two bending magnets, three solenoids, two quadrupoles, two magnetic steeres and three collimators. The beam is bent 90° through each bending magnet and then goes through a collimator to discard remaining unmoderated positrons. The optics provides an adjustable size and adjustable angular divergence beam, which is necessary for channeling and scattering experiments.

We installed a new image plate capable target chamber on this beam line. The beam goes through two collimators size 10, 0.2 mm placed 2 m apart to establish the angular divergence and beam size on the target. A movable microchannel plate is used before the target to monitor the beam size and check that there is no slit scattering. The (1 0 0) Au sample was mounted on a two axis (θ, φ) goniometer and a stereogram for the crystal was obtained by measuring the transmitted positrons yield in the forward direction over a small solid angle. A 2.8 MeV positrons beam of 1000 counts/s, spot size of 0.2 mm, and 0.3° angular divergence was focused on the gold sample. Then, the transmitted positrons hit an IP, which is mounted on a movable holder 10 cm behind the target to cover about a 15° half angle. The angular resolution of the beam on the IP is 0.3°.

The measurements were performed in the random and nominal ⟨1 0 0⟩ channeling direction. The random direction has been chosen from a point on a channeling stereogram 3.78° away from the ⟨1 0 0⟩ axis. The measured angular distributions of 2.8 MeV positrons behind a 1.67 μm Au crystal in the random and aligned ⟨1 0 0⟩ directions are shown in Figs. 4 and 5, respectively. The vertical represents an average over 2π azimuthal angle around the incident beam direction. The picture and the surface plot of the beam on the image plate are displayed in Figs. 6 and 7, respectively, for random and ⟨1 0 0⟩ direction showing a very large difference between random and aligned incident beam conditions.

3. Multiple scattering in random direction

For the following assume that the positron scattering in a crystal in the random direction is similar to that in a random amorphous material. It can then be described by multiple scattering theories in which the particle is considered to have a certain direction (θ) after being scattered a certain number of times with no correlation between the events. The multiple scattering of MeV positrons has been calculated using the Goudsmit–Saunderson multiple scattering theory which uses the aforementioned assumption [18,19] with the

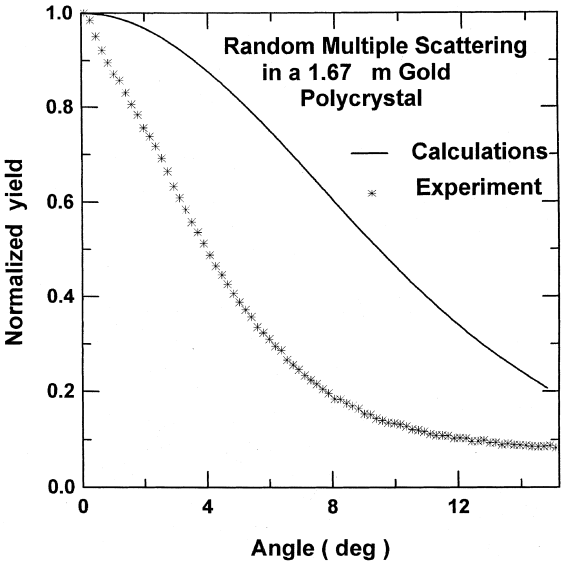

Fig. 4. Angular distribution of 2.8 MeV positrons behind 1.67 μm Au crystal. The solid line represents the calculated distribution. The dotted line represents the measured distribution in the random direction averaged around the incident beam direction.

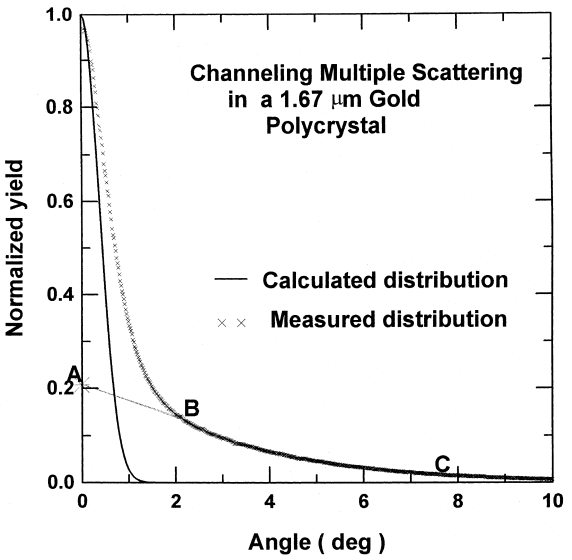

Fig. 5. Angular distribution of 2.8 MeV positrons behind 1.67 μm Au crystal in ⟨1 0 0⟩ direction. The solid line represents the calculated distribution. The dotted line represents the measured distribution averaged around the incident beam direction.

Thomas–Fermi potential. The distribution function is expressed as Legendre series,

$$F(\theta,t)\sin\theta\,\mathrm{d}\theta = \sum_{\ell=0}^{\infty}(\ell+0.5)\,\exp\left[-\int_0^t k_\ell(t)\,\mathrm{d}t\right] \times P_\ell(\cos\theta)\sin\theta\,\mathrm{d}\theta, \quad (1)$$

provided that the scattering is cylindrically symmetric, where

$$k_\ell(t) = 2\pi N\int_0^\pi \sigma(\theta,t)[1-P_\ell(\cos\theta)]\sin\theta\,\mathrm{d}\theta. \quad (2)$$

$F(\theta,t)$ represents the differential multiple scattering cross-section, θ is the total deviation from the origin direction, N the number of atoms per unit volume, $\sigma(\theta,t)$ the single scattering cross-section per unit solid angle and t the thickness of target. We used the Rutherford single scattering cross-section for an unscreened potential modified by a screening factor η based on the Thomas–Fermi potential and by a spin relativistic factor R [20].

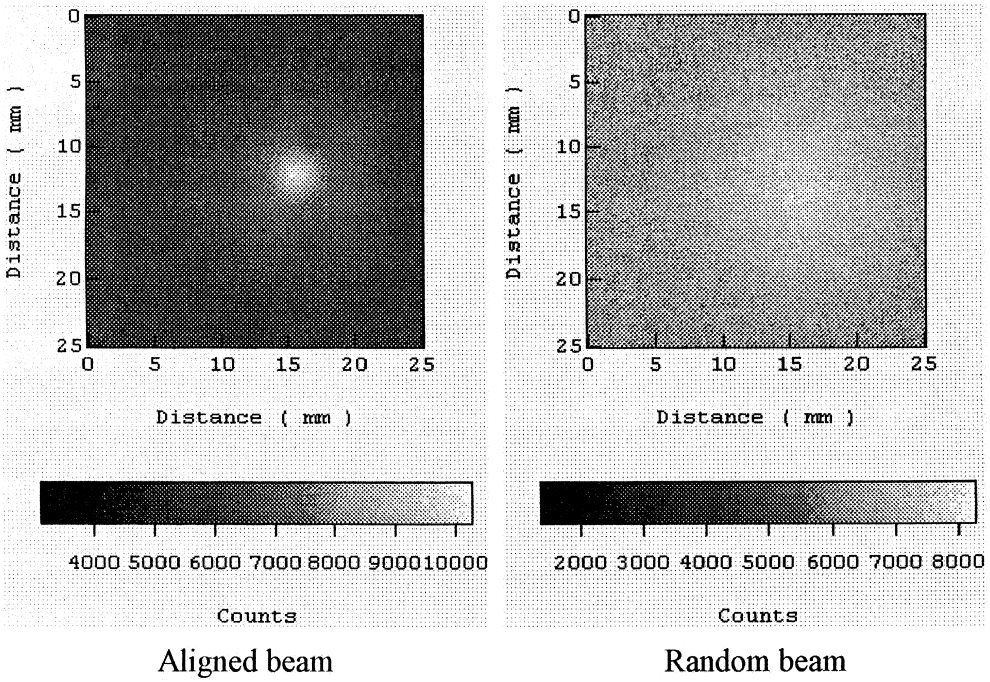

Fig. 6. Picture of the positron beam on the IP behind 1.67 μm Au crystal.

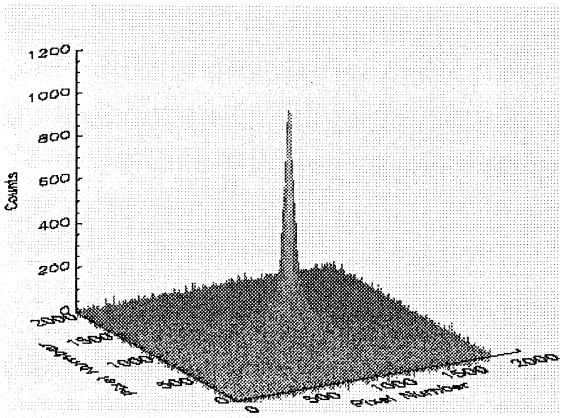

Aligned beam

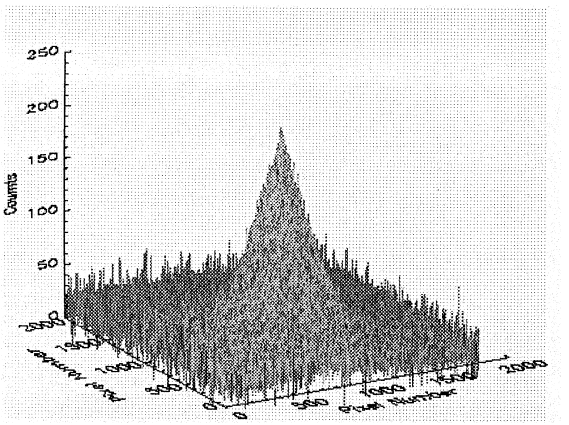

Random beam

Fig. 7. Surface plot of the positron beam behind 1.67 μm Au crystal each pixel represents angle of 0.019°.

$$\sigma_R = \frac{Z^2 e^4}{P^2 V^2 (1 + 2\eta - \cos\theta)^2} * R, \tag{3}$$

where P, V are the momentum and velocity of the particle, e the electron charge, Z the atomic number. Multiple scattering due to electronic collisions was considered but it is negligible.

The calculated angular distribution of 2.8 MeV positrons behind a 1.67 μm gold has been compared with the measured distribution in the random direction in Fig. 4. It is clear from the graph that neither the measured nor calculated distribution is Gaussian. The calculated distribution is much wider than the measured one by a factor of 2. However, we tested the calculation procedure in a previous work [20] for random materials. It showed a very good agreement with the experiment for electrons in Al at 2.25 MeV and a reasonable agreement for electrons in Cu at 2.25 MeV. The discrepancy between the experiment and the theory for the Au crystal may be accounted for crystal effects and inaccuracies in the scattering cross-section at high atomic numbers. The assumptions of cylindrically symmetric scattering and uncorrelated scattering are shared by all multiple scattering theories. These assumptions may fail when the atoms of the scatterer are distributed in some regular way as in crystals.

From a quantum mechanical point of view, interference effects associated with correlation between scattering may have a major role in the discrepancy between the experiments and the theories. This will be discussed in Section 4. Describing the screening by the Thomas–Fermi potential is not accurate for the high Z materials at small angles and may contribute to the discrepancy. Also, the single scattering cross-section is calculated from a potential assuming isolated atom while the particle in crystal experience a potential modified by the lattice structure.

4. Multiple scattering in the channeling direction

In the channeling direction, the positrons are steered into the open regions of the lattice by a series of gentle small angle scatterings due to the ordered structure of the crystal. Mostly they do not penetrate to the ion core region and nuclear contribution to the scattering are greatly reduced. They are however multiple scattered by the outer and valence electrons. The multiple scattering of channeled positrons due to electronic collisions can be given by [21]

$$\langle \mathrm{d}\Omega^2/\mathrm{d}z \rangle_{\mathrm{e}} = \frac{1}{PV\gamma} S_{\mathrm{e}} n_{\mathrm{e}}, \tag{4}$$

where Ω is the angular deviation due to electronic collisions, z the depth, P the positron momentum

and V the velocity, $\gamma = E/mc^2$, E the total positron energy. S_e the electronic stopping cross-section and n_e is the average electron density in the channel. It equals about 0.17 e/A^3 for $\langle 1\,0\,0\rangle$ gold. For relativistic velocities, S_e is given by [2]

$$S_e = \frac{2\pi e^4}{mV^2}\left[\log\frac{mV^2E}{2I^2(1-\beta^2)} - \left(2\sqrt{1-\beta^2} - 1 + \beta^2\right)\log 2 + 1 - \beta^2 + \frac{1}{8}\left(1-\sqrt{1-\beta^2}\right)^2\right], \quad (5)$$

where m is the electron mass, $\beta = V/c$, and $I = h\omega_p$, where ω_p the plasma frequency of the valence electron gas, $\omega_p^2 = (4\pi n_e e^2/m)$. Fig. 8 shows the predicted average deflection of 2.8 MeV positrons due to the scattering by valence electrons along $\langle 1\,0\,0\rangle$ in gold as a function of depth. The measured and the calculated angular distributions of 2.8 MeV channeled positrons behind a 1.67 μm Au sample in the $\langle 1\,0\,0\rangle$ axis direction are shown in Fig. 5. The calculated distribution is obtained for a perfect crystal by assuming a Gaussian distribution due to the multiple scattering by the valence electrons only and by taking into account the initial divergence 0.3 of the beam. The half width at half maximum of the measured distribution is about 0.9° which is also equal to the critical angle for channeling ψ_c [16].

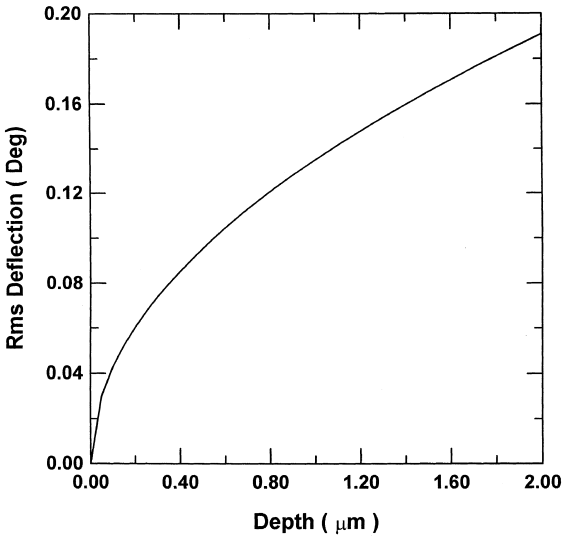

Fig. 8. Multiple scattering of the channeled positrons by valence electrons in Au crystal.

$$\psi_c = \frac{\psi_1}{\sqrt{2}}\left[\ln\left(\frac{ca}{\rho}\right)^2 + 1\right]^{1/2}, \quad (6)$$

$$\psi_1 = \sqrt{\frac{2Z_1Z_2e^2}{\frac{1}{2}PVd}}, \quad (7)$$

where Z_1e is the particle charge, Z_2 the atomic number of the target, P the momentum of the particle, and V the velocity, d the atomic spacing, ρ the transverse root mean square thermal vibration ($\rho = 123$ A° at 293 K° for gold), a the screening length, and c a constant equal to $\sqrt{3}$. It is possible to extract information about the dechanneling of the beam from the measured distribution by extrapolating the tail of the curve denoted by BC in Fig. 5 to point A and evaluating the ratio of the area under ABC to the total area. This gives approximately 50% dechanneling, consistent with the proton measurements mentioned earlier.

5. Quantum mechanical effects

In some exposures in the channeling direction, the size of the beam and its angular divergence were reduced to ensure angular resolution at the image plate better than 0.053° which is the (1 0 0) Bragg angle. Diffraction peaks were never observed. These are the first transmission channeling measurements of MeV positrons in gold. Transmission diffraction of positrons has been observed recently for thin silicon in [22]. The lack of diffraction peaks in our experiments may be explained by strong inelastic scattering. Due to energy transfer to electrons, the coherence of the positron wave function is destroyed, the diffraction peaks broaden and a continuous distribution appears. Blocking effects also were not observed in our measurements.

In electron diffraction by relatively thick crystals [23], the diffraction patterns are transformed by inelastic scattering, most of which occurs at

very small angles. These scattered electrons are rediffracted by the crystal and the resulting pattern is characterized by complex Kikuchi lines and bands and ring patterns. With increasing crystal thickness, the ring pattern predominates. Actually the crystal used in our measurements is very thick compared to all those used in existing measurements with electron microscopy.

Nonchanneled positrons travel in random directions, not parallel to an axis or plane, but the crystal structure can still have an effect on the scattering perhaps through interference which reinforces the forward scattering and leads to a strong maximum in the forward direction. It is an interesting question whether the lattice structure in a classical solution of the multiple scattering of positrons in crystals will give good agreement with the experiments for random multiple scattering. Classical binary collision calculations of the channeling angular yield for wide angle scattering have been performed [24]. Good agreement with the experimental results of Anderson et al. [25] was obtained. For small angle scattering the situation may be different.

For a single scattering, the classical orbital picture of collision seems to fail if the wavelength of the particle $\lambda\!\!\!^{-} = \hbar/mV$ is comparable to the collision length $b = 2Ze^2/mV^2$. This condition is illustrated by Bohr [3]:

$\kappa \gg 1$ for the valadity of classical orbital picture where, $\kappa = b/\lambda\!\!\!^{-}$.

For MeV positrons in gold κ is comparale to 1.

6. Conclusion

Our measurements demonstrate the utility of image plates as a quantitative position sensitive detector for positrons. The IP has the advantage of good sensitivity, very good linearity and wide dynamic range. Also the measurements represent the first for the multiple scattering of monoenergetic MeV positrons. There is a serious discrepancy between the experiment and the classical multiple scattering theory mostly likely due to crystal and quantum mechanics effects. It seems that the interference effect in crystals leads to an increase in the forward scattering. We suggest that detailed many beam calculations to describe forward multiple scattering yields far from channeling conditions may be very informative.

Acknowledgements

We would like to acknowledge Prof. John Spence and Paul Perkers for providing us with the image plates and processing them at Arizona State University, and for also useful discussions about the performance of the image plates. We also think N. Mori at Fuji Photo Film in Japan and Thomas Cowan at LLNL for useful discussions about the image plates. We would like to acknowledge Prof. Ejvind Bonderup at Aarhus University for his valuable discussions in positron scattering. The work was supported by US NSF under contract No. DMR 926 3610 and under the auspices of the US DOE by Lawrence Livermore National Laboratory under contract No. W-7405-ENG48.

References

[1] C.D. Zerby, F.L. Keller, Nucl. Sci. Engrg. 27 (1967) 190.
[2] H.A. Bethe, J.A. Askin, Experimental nuclear physics, in: E. Segré (Ed.), Passage of Radiation Through Matter, Vol. 1, 1933.
[3] N. Bohr, Mat. Fys. Medd. K. Dan. Selsk 18 (18) (1948).
[4] L.A. Kulchitsky, G.D. Latyshev, Phys. Rev. 61 (1942) 254.
[5] Hanson, Lanzl, Lyman, Scott, Phys. Rev. 84 (1951) 634.
[6] R. Haakenaaseen, A.W. Hunt, J.A. Golovchenko, R.H. Howell, F.A. Selim, K.G. Lynn, T.E. Cowan, L.V. Hau, Mat. Sci. Forum 255–257, in: Y.C. Jean, M. Eldrup, D.M. Schrader, R.N. West (Eds.), Proc. ICPA-11, 1997, p. 257.
[7] L.V. Hau, J.A. Golovchenko, R. Haakenaasen, A.W. Hunt, J.P. Peng, P. Asoka-Kumar, K.G. Lynn, M. Weinert, J.C. Palathingal, Nucl. Instr. and Meth. B 119 (1996) 30.
[8] J. Miyahara, K. Takahasi, Y. Amemiya, N. Kamiya, Y. Satow, Nucl. Instr. and Meth. A 246 (1986) 572.
[9] N. Mori, T. Oikawa, T. Katoh, J. Miyahara, Y. Harada, Ultamicroscopy 25 (1988) 195.
[10] N. Mori, T. Oikawa, Y. Harada, J. Miyahara, J. Electron Microsc. 39 (1990) 433.
[11] J.M. Zuo, M.R. McCaetney, J.H. Spence, Ultamicroscopy 66 (1996) 35.
[12] P.J. Schultz, K.G. Lynn, Rev. Mod. Phys. 60 (1988) 701.
[13] L. Katz, S. Penfold, Rev. Mod. Phys. 24 (1952) 28.
[14] L. Pages, E. Bertel, H. Joffre, L. Sklavenitis, Atomic Data 4 (1972) 1.

[15] M. Thomas, Nucl. Instr. and Meth. A 378 (1996) 598.
[16] L.C. Feldman, J.W. Mayer, S.T. Picraux, Materials Analysis by Ion Channeling, Academic Press, New York, 1982.
[17] D.W. Pashley, M.J. Stowell, Philos. Mag. 8 (1963) 160.
[18] S.G. Goudsmit, J.L. Saunderson, Phys. Rev. 57 (1940) 24.
[19] S.G. Goudsmit, J.L. Saunderson, Phys. Rev. 57 (1940) 36.
[20] F.A. Selim, J.A. Golovchenko, M. Abou Mandour, R. Howell, M.S. Abou Elwafa, Mat. Sci. Forum 255–257, in: Y.C. Jean, M. Eldrup, D.M. Schrader, R.N. West (Eds.), Proc. ICPA-11, 1977, p. 266.
[21] F.A. Selim, Ph.D. Thesis, Alexandria University, May 1999.
[22] R. Haakenaaseen, L. Vesteregaard Hau, J.A. Golovchenko, J.C. Palathingal, J.P. Peng, P. Asoka Kumar, K.G. Lynn, Phys. Rev. Lett. 75 (1995) 1650.
[23] S.L. Dudarev, L.M. Peng, Proc. R. Soc. Lond. 440 (1993) 117.
[24] V.V. Kudrin, Yu.A. Timoshnikov, S.A. Vorobew, Phys. Stat. Solids B 56 (1973) 409.
[25] J.U. Anderson, W.M. Augustyniak, E. Uggerhøj, Phys. Rev. B 3 (1971) 705.